AIP Journal of Applied Physics

Modeling of resonant magneto-electric effect in a magnetostrictive and piezoelectric laminate composite structure coupled by a bonding material

D. Hasanyan, Y. Wang, J. Gao, M. Li, Y. Shen, J. Li, and D. Viehland

Citation: Journal of Applied Physics **112**, 064109 (2012); doi: 10.1063/1.4752271
View online: http://dx.doi.org/10.1063/1.4752271
View Table of Contents: http://scitation.aip.org/content/aip/journal/jap/112/6?ver=pdfcov
Published by the AIP Publishing

Modeling of resonant magneto-electric effect in a magnetostrictive and piezoelectric laminate composite structure coupled by a bonding material

D. Hasanyan,[a] Y. Wang, J. Gao, M. Li, Y. Shen, J. Li, and D. Viehland
Materials Science and Engineering, Virginia Tech, Blacksburg, Virginia 24061, USA

(Received 8 June 2012; accepted 9 August 2012; published online 18 September 2012)

The harmonic magneto-electro-elastic vibration of a thin laminated composite was considered. A theoretical model, including shear lag and vibration effects was developed for predicting the magneto-electric (ME) effect in a laminate composite consisting of magnetostrictive and piezoelectric layers. To avoid bending, we assumed that the composite was geometrically symmetric. For finite length symmetrically fabricated laminates, we derived the dynamic strain-stress field and ME coefficients, including shear lag and vibration effects for several boundary conditions. Parametric studies are presented to evaluate the influences of material properties and geometries on the strain distribution and the ME coefficient. Analytical expressions indicate that the shear lag and the vibration frequency strongly influence the strain distribution in the laminates and these effects strongly influence the ME coefficients. © *2012 American Institute of Physics*. [http://dx.doi.org/10.1063/1.4752271]

I. INTRODUCTION

Multiferroics are a special class of materials that have attracted much attention because of their potential for enhanced functionality in sensors and devices.[1,2] For the past fifty years, magnetoelectric (ME) materials have evolved from single phase compounds, to particulate composites, and finally to laminate composites.[1–10] The remarkably higher ME effects observed in laminate composites are produced by mechanically coupling continuous magnetostrictive and piezoelectric layers. For example, a ME voltage coefficient of 22 V/cm Oe under a low H_{bias} of 2 Oe was reported by authors.[3,11] While several models for laminate ME composites exist, these typically over predict the experimental results significantly. This paper provides an explanation for this discrepancy and a corresponding analytical model validated with experimental results.

Authors[12] provided an analytical foundation for static ME laminate composites. However, this theoretical approach gave a huge disagreement with experiments, because of an assumption that all field functions are homogeneously distributed throughout the composite. To eliminate disagreement between analysis and experiments, authors[13] proposed a model that include interface coupling parameter k to account for sliding boundary conditions at the ME laminate interfaces. While this provided an approach to better correlate theoretical analysis with the test data, it is unlikely that interface slip occurs at well-bonded continuous interfaces. The magnitude of the ME effect significantly increases in the region of the electromechanical resonance.[8,14] Theory of this phenomenon was developed and experimentally verified using samples in the form of disks and plates. A theoretical model that predicts very strong ME interactions at magneto acoustic resonance in single-crystal ferrite-piezoelectric bilayer is discussed in Ref. 15.

Another possible influence on ME laminates that has not been well considered is the shear lag effect. Authors[16] presented a modified shear lag approach to predict load transfer between piezoelectric actuators and an elastic substructure, i.e., electromechanical coupling. The corresponding stress and strain distribution in the piezoelectric laminate composite were studied and confirmed by experiments. Modeling of static shear lag and demagnetization effects in ME laminate composites was proposed by authors.[17] However, a dynamic shear lag yet has not applied to electro-magneto-mechanically coupled ME composites.

In this paper, an analytical model is proposed to predict the dynamic response of a laminate ME composite. Shear lag analysis, along with geometrical and vibration characteristics, is incorporated to provide spatial solutions for strain, magnetic field variations, as well as effective ME voltage coefficient.

II. MODEL AND CONSTITUITIVE EQUATIONS FOR A THREE LAYER ME LAMINATE COMPOSITE CONSIDERING AN INTERLAYER BONDING MATERIAL

We consider a tri-layer laminated structure in the shape of a bar with a length $2L$ and a total thickness of $h = 2h_b + h_p + 2h_m$ ($L \gg h$). The specimen is polarized along the longitudinal (L) direction to the planes of the contacts (i.e., the x_3-axis). Static (magnetic bias) and alternating magnetic fields were applied along the L direction and across the planes of the contacts ($\vec{H}_{appl}$). Magnetostrictive and piezoelectric layers are bonded together with a bonding material-layer of a finite thickness h_b and of finite elastic properties G_b. If the thickness of the bonding layer $h_b \to 0$ or shear modulus $G_b \to \infty$, we can assume that the magnetostrictive and piezoelectric layers are perfectly bonded together. A schematic view of the considered problem is shown in Figure 1.

Due to magnetostriction, an alternating magnetic field induces vibrations in the magnetostrictive layers, which propagate both across and along the specimen. Our further

[a]Author to whom correspondence should be addressed. Electronic mail: dhasanya@vt.edu.

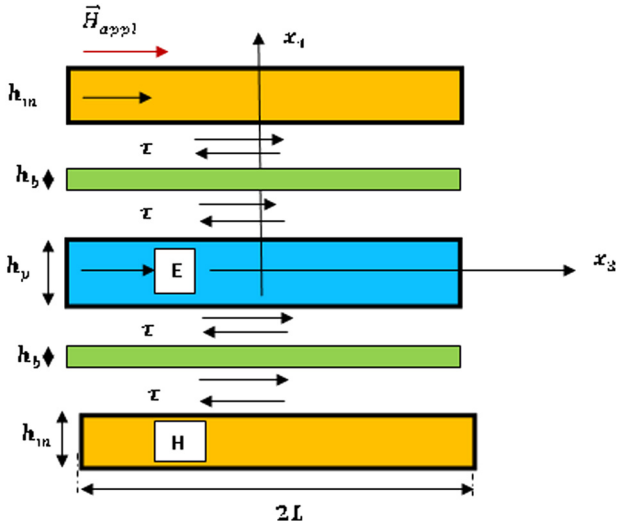

FIG. 1. Magneto electric laminated composite. The arrow's indicates the direction of polarization, applied magnetic field, and shear stress between two phases.

considerations will be a case for only bulk vibrations propagating along the plane of the specimen (i.e., no bending). Mechanical vibrations of the magnetostrictive medium are transferred to the piezoelectric component via mechanical bonding, wherein an electric field is induced by the piezoelectric effect.

We assume further that the total thickness $(h = 2h_b + h_p + 2h_m)$ and width W of the specimen are much smaller than its length $2L$ and the stresses on its surfaces can be assumed to be equal to zero. Since the plate is thin and narrow, i.e., 1D strain-displacement state, we can also assume that the stress components T_1 and T_2 are equal to zero not only on the surface but also in the bulk: Only the T_3 tensor component is different from zero. We also assume that only the E_3 and H_3 components of the electric and magnetic fields are non-zero. Accordingly, the equations for the strain tensor S_{3m} and the magnetic induction B_3 in the magnetostrictive layers and for the strain tensor S_{3p} and electric field inductance D_{3p} in the piezoelectric ones for the case of a longitudinal field orientation have the following form:[18,19]

$$\begin{aligned} S_{3m} &= s_{33}^{M} T_{3m} + q_{33} H_3, \\ B_3 &= q_{33} T_{3p} + \mu_{33} H_3, \\ S_{3p} &= s_{33}^{P} T_{3p} + d_{33} E_3, \\ D_3 &= d_{33} T_{3p} + \varepsilon_{33} E_3, \end{aligned} \tag{1}$$

where s_{33}^{M} and s_{33}^{P} are the elastic compliance tensors components of the magnetostrictive and piezoelectric layers, respectively; ε_{33} and μ_{33} are the relative dielectric and magnetic permeability tensor components of the piezoelectric and piezomagnetic layers respectively; and d_{33} and q_{33} are the piezoelectric and piezomagnetic coefficients, respectively. Note that for the case of transverse orientation of $H_1(E_1)$, the functions q_{33} (d_{33}) and $H_3(E_3)$ will be replaced by q_{31} (d_{31}) and H_1 (E_1) in Eq. (1), respectively.

Shear lag analysis then assumes a pure shear in the bonding layer and a pure extension in both the piezoelectric and magnetostrictive layers. The 1D strain-displacement relationships are thus

$$S_{3m} = \frac{\partial u_{3m}}{\partial x_3}, \quad S_{3p} = \frac{\partial u_{3p}}{\partial x_3}, \quad \gamma_b = \frac{u_{3p} - u_{3m}}{\mathrm{h_b}}, \tag{2}$$

where γ_b denotes the shear strain in the bonding layer, which is related to shear stress by an isotropic stress-strain relationship $\tau = G_b \gamma_b$ (see Refs. 16 and 17). For the pure extension assumption, as illustrated in the free body diagram of Fig. 1, the force equilibrium equations for the representative elements are given by

$$\begin{aligned} \rho_m \frac{\partial^2 u_{3m}}{\partial t^2} &= \frac{\partial T_{3m}}{\partial x_3} + \frac{\tau}{\mathrm{h_m}}, \\ \rho_p \frac{\partial^2 u_{3p}}{\partial t^2} &= \frac{\partial T_{3p}}{\partial x_3} - \frac{2\tau}{\mathrm{h_p}}, \end{aligned} \tag{3}$$

where ρ_m and ρ_p are densities of the magnetostrictive and piezoelectric phases, respectively. Equations (1)–(3) should be considered, along with Maxwell's magnetostatic and electrostatic equations in magnetostrictive and piezoelectric layers, given as

$$\begin{aligned} div\,\vec{B} &= 0, \quad rot\,\vec{H} = 0, \\ div\,\vec{D} &= 0, \quad t\vec{E} = 0. \end{aligned} \tag{4}$$

Equations (1)–(3) are written under the assumption that all field components do not vary through the thickness and width directions of the laminate composites.

III. GENERAL AND SPECIFIC SOLUTIONS FOR MODEL

First, we must set up the equations. Using the constitutive equations of Eq. (1), the bonding stress-strain relations of $\tau = G_b \gamma_b$, the strain-displacement equations of Eq. (2), the equations of motions of Eq. (3), and Maxwell's equations of Eq. (4), two coupled partial differential equations can be derived in terms of the displacements $u_{3m}(x_3, t)$ and $u_{3p}(x_3, t)$

$$\rho_m \frac{\partial^2 u_{3m}}{\partial t^2} = \frac{\mu_{33}}{s_{33}^{M}\mu_{33} - q_{33}^2} \frac{\partial^2 u_{3m}}{\partial x_3^2} + \frac{G_b}{\mathrm{h_m h_b}} [u_{3p} - u_{3m}], \tag{5}$$

$$\rho_p \frac{\partial^2 u_{3p}}{\partial t^2} = \frac{\varepsilon_{33}}{s_{33}^{P}\varepsilon_{33} - d_{33}^2} \frac{\partial^2 u_{3p}}{\partial x_3^2} - \frac{2G_b}{\mathrm{h_p h_b}} [u_{3p} - u_{3m}]. \tag{6}$$

Assuming

$$\begin{aligned} &u_{3m}(x_3, t) = u_m(x_3) e^{i\omega t}, \quad u_{3p}(x_3, t) = u_p(x_3) e^{i\omega t}, \\ &H_3(x_3, t) = H_3 e^{i\omega t} \text{ and } E_3(x_3, t) = E_3 e^{i\omega t} \end{aligned}$$

from Eqs. (5) and (6), we can derive

$$\frac{\omega^2}{\Omega_m^2} u_m(z) = \alpha_m \frac{d^2 u_{3m}}{dz^2} + \beta_m [u_{3p} - u_{3m}], \tag{7}$$

$$\frac{\omega^2}{\Omega_p^2}u_p(z) = \alpha_p \frac{d^2u_{3m}}{dz^2} - \alpha\beta_p[u_{3p} - u_{3m}]. \quad (8)$$

In Eqs. (7) and (8), we introduced following nondimensional parameters:

$$\Omega_m^2 = \frac{1}{\rho_m s_{33}^M L}, \quad \Omega_p^2 = \frac{1}{\rho_p s_{33}^P L}, \quad \alpha_m = \frac{\mu_{33}s_{33}^M}{s_{33}^M\mu_{33} - q_{33}^2},$$

$$\alpha_p = \frac{\varepsilon_{33}s_{33}^P}{s_{33}^P\varepsilon_{33} - d_{33}^2}, \quad \beta_m = \frac{G_b s_{33}^M}{\mathrm{t_m t_b}},$$

$$\beta_p = \frac{G_b s_{33}^P}{\mathrm{t_p t_b}}, \quad \alpha = 2, \quad z = x_3/L, \quad \mathrm{t_p} = \mathrm{h_p/L},$$

$$\mathrm{t_b} = \mathrm{h_b/L}, \quad \mathrm{t_m} = \mathrm{h_m/L}.$$

Second, we must find the general solutions of the equations. The general solutions of the system of Eqs. (7) and (8) can be expressed in the following two forms under different conditions:

(1) If $\omega < \sqrt{\alpha\beta_p\Omega_p^2 + \beta_m\Omega_m^2} = \omega_0$, then

$$\begin{pmatrix} u_m(z) \\ u_p(z) \end{pmatrix} = \begin{pmatrix} 1 \\ \tilde{\lambda}_1 \end{pmatrix} A_1 \sin\gamma_1 z + \begin{pmatrix} 1 \\ \tilde{\lambda}_1 \end{pmatrix} A_2 \cos\gamma_1 z + \begin{pmatrix} 1 \\ \tilde{\lambda}_2 \end{pmatrix} A_3 \sin\gamma_2 z + \begin{pmatrix} 1 \\ \tilde{\lambda}_2 \end{pmatrix} A_4 \cos\gamma_2 z, \quad (9)$$

(2) If $\omega > \sqrt{\alpha\beta_p\Omega_p^2 + \beta_m\Omega_m^2} = \omega_0$, then

$$\begin{pmatrix} u_m(z) \\ u_p(z) \end{pmatrix} = \begin{pmatrix} 1 \\ \tilde{\lambda}_1 \end{pmatrix} A_1 \sin\gamma_1 z + \begin{pmatrix} 1 \\ \tilde{\lambda}_1 \end{pmatrix} A_2 \cos\gamma_1 z + \begin{pmatrix} 1 \\ \tilde{\lambda}_2 \end{pmatrix} A_3 \sinh\gamma_2 z + \begin{pmatrix} 1 \\ \tilde{\lambda}_2 \end{pmatrix} A_4 \cosh\gamma_2 z. \quad (10)$$

In Eqs. (9) and (10), we introduced the following notations:

$$\tilde{\lambda}_k = \frac{1}{\beta_m}\left[\frac{\omega^2}{\Omega_m^2} - \alpha_m\lambda_k + \beta_m\right], \gamma_k = \sqrt{|\lambda_k|}. \quad (11)$$

$$\lambda_k = \frac{1}{2\alpha_m\alpha_p}\left\{\alpha_m\left(\alpha\beta_p - \frac{\omega^2}{\Omega_p^2}\right) + \alpha_p\left(\beta_m - \frac{\omega^2}{\Omega_m^2}\right) + (-1)^k\sqrt{\left[\alpha_m\left(\alpha\beta_p - \frac{\omega^2}{\Omega_p^2}\right) + \alpha_p\left(\beta_m - \frac{\omega^2}{\Omega_m^2}\right)\right]^2 + 4\alpha_m\alpha_p\alpha\beta_p\beta_m}\right\}, \quad (k = 1,2). \quad (12)$$

From Eq. (12), we can show that, $\lambda_1 < 0$ for $0 \le \omega < \infty$, $\lambda_2 > 0$ for $0 \le \omega \le \omega_0$, and $\lambda_2 < 0$ for $\omega_0 < \omega < \infty$.

Third, we must apply boundary conditions to get specific solutions. Four boundary conditions can now be applied to determine the four unknown constants of $A_i(i = 1,2,3,4)$. It should be noted that the magnetostrictive and piezoelectric strains $q_{33}H_3$ and $d_{33}E_3$ do not appear explicitly neither in the motion equations of Eqs. (5) and (6) nor in the solutions of Eqs. (9) and (10), but they enter into the solutions through the boundary conditions. We next have to examine the following three particular boundary conditions applied to the edges of the laminated composite: case (I) both ends are traction free; case (II) one end is clamped and the other end is traction free; case (III) both ends are traction free of the magnetostrictive layers and zero strains on both ends of the piezoelectric layer.

Using the constitutive equations of Eq. (1) and the strain-displacement relations of Eq. (2), the boundary conditions for the above mentioned three cases can be expressed in terms of their displacements as follows:

Case (I)
For $z = \pm 1$

$$\frac{du_p(z)}{dz} = d_{33}E_3 \quad \text{and} \quad \frac{du_m(z)}{dz} = \beta q_{33}H_3. \quad (13)$$

Case (II)
For $z = -1$

$$u_p(z) = 0 \quad \text{and} \quad u_m(z) = 0. \quad (14)$$

When $z = +1$

$$\frac{du_p(z)}{dz} = d_{33}E_3, \quad \text{and} \quad \frac{du_m(z)}{dz} = \beta q_{33}H_3. \quad (15)$$

Case (III)
For $z = \pm 1$

$$\frac{du_p(z)}{dz} = 0 \quad \text{and} \quad \frac{du_m(z)}{dz} = \beta q_{33}H_3. \quad (16)$$

In Eqs. (13), (15), and (16), we introduced a demagnetization coefficient of $\beta = 1 - N_d(\mu_{33} - 1)$, where N_d is a demagnetization factor which is a function of sample geometry. The parameter β belongs to the interval of $0 < \beta < 1$ (see Refs. 17 and 20). If, for ferromagnetic plates, $\mathrm{t_m} < 10^{-1}$, then $\beta \approx 1$.

Using the general solutions of Eq. (9) or (10) and the boundary conditions for these cases mentioned above, we can uniquely determine the unknown coefficients $A_i(i = 1,2,3,4)$. Without going into details, the specific solutions for Eq. (9) or (10) can be expressed as follows:

Case (I)
If $\omega < \sqrt{\alpha\beta_p\Omega_p^2 + \beta_m\Omega_m^2} = \omega_0$, then

$$u_m(z) = \frac{\tilde{\lambda}_2\beta q_{33}H_3 - d_{33}E_3}{\tilde{\lambda}_2 - \tilde{\lambda}_1}\frac{\sin\gamma_1 z}{\gamma_1\cos\gamma_1} + \frac{d_{33}E_3 - \tilde{\lambda}_1\beta q_{33}H_3}{\tilde{\lambda}_2 - \tilde{\lambda}_1}\frac{\sinh\gamma_2 z}{\gamma_2\cosh\gamma_2},$$

$$u_p(z) = \tilde{\lambda}_1 \frac{\tilde{\lambda}_2 \beta q_{33} H_3 - d_{33} E_3}{\tilde{\lambda}_2 - \tilde{\lambda}_1} \frac{\sin\gamma_1 z}{\gamma_1 \cos\gamma_1} + \tilde{\lambda}_2 \frac{d_{33} E_3 - \tilde{\lambda}_1 \beta q_{33} H_3}{\tilde{\lambda}_2 - \tilde{\lambda}_1} \frac{\sin h\gamma_2 z}{\gamma_2 \cos h\gamma_2},$$

If $\omega > \sqrt{\alpha\beta_p\Omega_p^2 + \beta_m\Omega_m^2} = \omega_0$, then

$$u_m(z) = \frac{\tilde{\lambda}_2 \beta q_{33} H_3 - d_{33} E_3}{\tilde{\lambda}_2 - \tilde{\lambda}_1} \frac{\sin\gamma_1 z}{\gamma_1 \cos\gamma_1} + \frac{d_{33} E_3 - \tilde{\lambda}_1 \beta q_{33} H_3}{\tilde{\lambda}_2 - \tilde{\lambda}_1} \frac{\sin\gamma_2 z}{\gamma_2 \cos\gamma_2},$$

$$u_p(z) = \tilde{\lambda}_1 \frac{\tilde{\lambda}_2 \beta q_{33} H_3 - d_{33} E_3}{\tilde{\lambda}_2 - \tilde{\lambda}_1} \frac{\sin\gamma_1 z}{\gamma_1 \cos\gamma_1} + \tilde{\lambda}_2 \frac{d_{33} E_3 - \tilde{\lambda}_1 \beta q_{33} H_3}{\tilde{\lambda}_2 - \tilde{\lambda}_1} \frac{\sin\gamma_2 z}{\gamma_2 \cos\gamma_2}.$$

Case (II)

If $\omega < \sqrt{\alpha\beta_p\Omega_p^2 + \beta_m\Omega_m^2} = \omega_0$, then

$$u_m(z) = \frac{[\tilde{\lambda}_2 \beta q_{33} H_3 - d_{33} E_3]}{\tilde{\lambda}_2 - \tilde{\lambda}_1} \frac{\sin\gamma_1 (z+1)}{\gamma_1 \cos 2\gamma_1} + \frac{[d_{33} E_3 - \tilde{\lambda}_1 \beta q_{33} H_3]}{\tilde{\lambda}_2 - \tilde{\lambda}_1} \frac{\sin h\gamma_2 (z+1)}{\gamma_2 \cos h2\gamma_2},$$

$$u_p(z) = \tilde{\lambda}_1 \frac{[\tilde{\lambda}_2 \beta q_{33} H_3 - d_{33} E_3]}{\tilde{\lambda}_2 - \tilde{\lambda}_1} \frac{\sin\gamma_1 (z+1)}{\gamma_1 \cos 2\gamma_1} + \tilde{\lambda}_2 \frac{[d_{33} E_3 - \tilde{\lambda}_1 \beta q_{33} H_3]}{\tilde{\lambda}_2 - \tilde{\lambda}_1} \frac{\sin h\gamma_2 (z+1)}{\gamma_2 \cos h2\gamma_2}.$$

If $\omega > \sqrt{\alpha\beta_p\Omega_p^2 + \beta_m\Omega_m^2} = \omega_0$, then

$$u_m(z) = \frac{\tilde{\lambda}_2 \beta q_{33} H_3 - d_{33} E_3}{\tilde{\lambda}_2 - \tilde{\lambda}_1} \frac{\sin\gamma_1 z}{\gamma_1 \cos\gamma_1} + \frac{d_{33} E_3 - \tilde{\lambda}_1 \beta q_{33} H_3}{\tilde{\lambda}_2 - \tilde{\lambda}_1} \frac{\sin\gamma_2 (z+1)}{\gamma_2 \cos 2\gamma_2},$$

$$u_p(z) = \tilde{\lambda}_1 \frac{\tilde{\lambda}_2 \beta q_{33} H_3 - d_{33} E_3}{\tilde{\lambda}_2 - \tilde{\lambda}_1} \frac{\sin\gamma_1 (z+1)}{\gamma_1 \cos 2\gamma_1} + \tilde{\lambda}_2 \frac{d_{33} E_3 - \tilde{\lambda}_1 \beta q_{33} H_3}{\tilde{\lambda}_2 - \tilde{\lambda}_1} \frac{\sin\gamma_2 (z+1)}{\gamma_2 \cos 2\gamma_2}.$$

Case (III)

If $\omega < \sqrt{\alpha\beta_p\Omega_p^2 + \beta_m\Omega_m^2} = \omega_0$, then

$$u_m(z) = \frac{\beta q_{33} H_3}{\tilde{\lambda}_2 - \tilde{\lambda}_1} \left\{ \tilde{\lambda}_2 \frac{\sin\gamma_1 z}{\gamma_1 \cos\gamma_1} - \tilde{\lambda}_1 \frac{\sin h\gamma_2 z}{\gamma_2 \cos h\gamma_2} \right\},$$

$$u_p(z) = \tilde{\lambda}_1 \frac{\tilde{\lambda}_2 \beta q_{33} H_3}{\tilde{\lambda}_2 - \tilde{\lambda}_1} \left\{ \frac{\sin\gamma_1 z}{\gamma_1 \cos\gamma_1} - \frac{\sin h\gamma_2 z}{\gamma_2 \cos h\gamma_2} \right\}.$$

If $\omega > \sqrt{\alpha\beta_p\Omega_p^2 + \beta_m\Omega_m^2} = \omega_0$, then

$$u_m(z) = \frac{\beta q_{33} H_3}{\tilde{\lambda}_2 - \tilde{\lambda}_1} \left\{ \tilde{\lambda}_2 \frac{\sin\gamma_1 z}{\gamma_1 \cos\gamma_1} - \tilde{\lambda}_1 \frac{\sin\gamma_2 z}{\gamma_2 \cos\gamma_2} \right\},$$

$$u_p(z) = \tilde{\lambda}_1 \frac{\tilde{\lambda}_2 \beta q_{33} H_3}{\tilde{\lambda}_2 - \tilde{\lambda}_1} \left\{ \frac{\sin\gamma_1 z}{\gamma_1 \cos\gamma_1} - \frac{\sin\gamma_2 z}{\gamma_2 \cos\gamma_2} \right\}.$$

IV. CALCULATION OF ME COEFFICIENT

The magneto-electric coupling coefficient α_{ME} can be determined under the open circuit condition of

$$I = \int\int \frac{dD_3}{dt} dS = 0, \tag{17}$$

where the integral is evaluated over the surface S of electrodes.

Using the constitutive equation of Eq. (1), condition (17) can be rewritten as

$$\left[\varepsilon_{33} - \frac{d_{33}^2}{s_{33}^P}\right] E_3 = -\frac{1}{2} \frac{d_{33}}{s_{33}^P} [u_p(-1) - u_p(+1)]. \tag{18}$$

Defining $\alpha_{ME} = \frac{E_3}{H_3}$, from Eq. (18), we can then derive the following ME coupling coefficients for the identified three cases

Case (I)

If $\omega < \sqrt{\alpha\beta_p\Omega_p^2 + \beta_m\Omega_m^2} = \omega_0$, then

$$\alpha_{ME}^I = \frac{\beta q_{33} d_{33}}{s_{33}^P \varepsilon_{33}} \frac{\tilde{\lambda}_1 \tilde{\lambda}_2}{\tilde{\lambda}_1 - \tilde{\lambda}_2} \frac{1}{\Delta_I} \left\{ \frac{tg\gamma_1}{\gamma_1} - \frac{th\gamma_2}{\gamma_2} \right\}, \tag{19}$$

where $\Delta_I = 1 - \frac{d_{33}^2}{s_{33}^P \varepsilon_{33}} \left\{ 1 - \frac{\tilde{\lambda}_1}{\tilde{\lambda}_1 - \tilde{\lambda}_2} \frac{tg\gamma_1}{\gamma_1} + \frac{\tilde{\lambda}_2}{\tilde{\lambda}_1 - \tilde{\lambda}_2} \frac{th\gamma_2}{\gamma_2} \right\}$.

If $\omega > \sqrt{\alpha\beta_p\Omega_p^2 + \beta_m\Omega_m^2} = \omega_0$, then

$$\alpha_{ME}^I = \frac{\beta q_{33} d_{33}}{s_{33}^P \varepsilon_{33}} \frac{\tilde{\lambda}_1 \tilde{\lambda}_2}{\tilde{\lambda}_1 - \tilde{\lambda}_2} \frac{1}{\Delta_I} \left\{ \frac{tg\gamma_1}{\gamma_1} - \frac{tg\gamma_2}{\gamma_2} \right\}, \tag{20}$$

where $\Delta_I = 1 - \frac{d_{33}^2}{s_{33}^P \varepsilon_{33}} \left\{ 1 - \frac{\tilde{\lambda}_1}{\tilde{\lambda}_1 - \tilde{\lambda}_2} \frac{tg\gamma_1}{\gamma_1} + \frac{\tilde{\lambda}_2}{\tilde{\lambda}_1 - \tilde{\lambda}_2} \frac{tg\gamma_2}{\gamma_2} \right\}$.

Case (II)

If $\omega < \sqrt{\alpha\beta_p\Omega_p^2 + \beta_m\Omega_m^2} = \omega_0$, then

$$\alpha_{ME}^I = \frac{\beta q_{33} d_{33}}{s_{33}^P \varepsilon_{33}} \frac{\tilde{\lambda}_1 \tilde{\lambda}_2}{\tilde{\lambda}_1 - \tilde{\lambda}_2} \frac{1}{\Delta_{II}} \left\{ \frac{tg2\gamma_1}{2\gamma_1} - \frac{th2\gamma_2}{2\gamma_2} \right\}, \tag{21}$$

where $\Delta_{II} = 1 - \frac{d_{33}^2}{s_{33}^P \varepsilon_{33}} \left\{ 1 - \frac{\tilde{\lambda}_1}{\tilde{\lambda}_1 - \tilde{\lambda}_2} \frac{tg2\gamma_1}{2\gamma_1} + \frac{\tilde{\lambda}_2}{\tilde{\lambda}_1 - \tilde{\lambda}_2} \frac{th2\gamma_2}{2\gamma_2} \right\}$.

If $\omega > \sqrt{\alpha\beta_p\Omega_p^2 + \beta_m\Omega_m^2} = \omega_0$, then

$$\alpha_{ME}^I = \frac{\beta q_{33} d_{33}}{s_{33}^P \varepsilon_{33}} \frac{\tilde{\lambda}_1 \tilde{\lambda}_2}{\tilde{\lambda}_1 - \tilde{\lambda}_2} \frac{1}{\Delta_{II}} \left\{ \frac{tg\gamma_1}{\gamma_1} - \frac{tg\gamma_2}{\gamma_2} \right\}, \tag{22}$$

where $\Delta_{II} = 1 - \frac{d_{33}^2}{s_{33}^P \varepsilon_{33}} \left\{ 1 - \frac{\tilde{\lambda}_1}{\tilde{\lambda}_1 - \tilde{\lambda}_2} \frac{tg2\gamma_1}{2\gamma_1} + \frac{\tilde{\lambda}_2}{\tilde{\lambda}_1 - \tilde{\lambda}_2} \frac{tg2\gamma_2}{2\gamma_2} \right\}$.

Case (III)

If $\omega < \sqrt{\alpha\beta_p\Omega_p^2 + \beta_m\Omega_m^2} = \omega_0$, then

$$\alpha_{ME}^I = \frac{\beta q_{33} d_{33}}{s_{33}^P \varepsilon_{33}} \frac{\tilde{\lambda}_1 \tilde{\lambda}_2}{\tilde{\lambda}_1 - \tilde{\lambda}_2} \frac{1}{\Delta_{III}} \left\{ \frac{tg\gamma_1}{\gamma_1} - \frac{th\gamma_2}{\gamma_2} \right\}, \quad (23)$$

where $\Delta_{III} = 1 - \frac{d_{33}^2}{s_{33}^P \varepsilon_{33}}$

If $\omega > \sqrt{\alpha\beta_p\Omega_p^2 + \beta_m\Omega_m^2} = \omega_0$, then

$$\alpha_{ME}^I = \frac{\beta q_{33} d_{33}}{s_{33}^P \varepsilon_{33}} \frac{\tilde{\lambda}_1 \tilde{\lambda}_2}{\tilde{\lambda}_1 - \tilde{\lambda}_2} \frac{1}{\Delta_{III}} \left\{ \frac{tg\gamma_1}{\gamma_1} - \frac{tg\gamma_2}{\gamma_2} \right\}, \quad (24)$$

where $\Delta_{III} = 1 - \frac{d_{33}^2}{s_{33}^P \varepsilon_{33}}$.

From Eqs. (19)–(24) for the ME coefficient, it follows at the frequencies where $\Delta_i = 0 (i = I, II, III)$ that there is resonant increase in $\alpha_{ME}^i (i = I, II, III)$. Next, we need to consider some particular cases for these solutions.

(a) Particular case of low frequency ME coefficients with an account of shear-lag effect (i.e., static shear-lag).

The low frequency ME coefficient can be derived assuming $\omega \to 0$ in Eqs. (19)–(24). In this case, it is easy to see that $\tilde{\lambda}_1 = 1$, $\tilde{\lambda}_2 = 1 - \frac{\alpha_m}{\beta_m}\lambda_2(0)$, and $\lambda_2(0) = \frac{\alpha\beta_m}{\alpha_p} + \frac{\beta_p}{\alpha_m} = \frac{G_b s_{33}^M}{t_b}\left(\frac{\alpha}{\alpha_p}\frac{1}{t_m} + \frac{s_{33}^P}{\alpha_m s_{33}^M t_p}\right) = \kappa^2\varsigma^2$, where $= \sqrt{\frac{G_b s_{33}^M}{t_b}}$, $\varsigma = \sqrt{\frac{\alpha}{\alpha_p}\frac{1}{t_m} + \frac{s_{33}^P}{\alpha_m s_{33}^M t_p}}$, $\lambda_1(0) = 0$, $\gamma_1 = 0$, and $\gamma_2 = \sqrt{\lambda_2(0)} = \gamma_{20}$. For example, the ME coefficient of case (II) can then be simplified to

$$\alpha_{ME}^{II} = -\frac{\beta q_{33} d_{33}}{s_{33}^P \varepsilon_{33}} \frac{1}{\Delta_{II}} \frac{\alpha\beta_p\alpha_m}{\alpha_p\beta_m + \alpha\beta_p\alpha_m} \left\{ 1 - \frac{th2\kappa\varsigma}{2\kappa\varsigma} \right\}, \quad (25)$$

where, $\Delta_{II} = 1 - \frac{d_{33}^2}{s_{33}^P \varepsilon_{33}} \left\{ 1 - \frac{\alpha_p}{\alpha_p + \alpha\eta\alpha_m} + \frac{\alpha\eta\alpha_m}{\alpha_p + \alpha\eta\alpha_m} \frac{th2\kappa\varsigma}{2\kappa\varsigma} \right\}$.

This case is consistent with the results of authors.[17] In addition to $\omega \to 0$, if we also assume perfect bonding between layers $\left(\text{i.e., } \kappa = \sqrt{\frac{G_b s_{33}^M}{t_b}} \to \infty\right)$, then from Eq. (25), we can obtain the following expression:

$$\alpha_{ME}^{II} = -\frac{\beta q_{33} d_{33}}{s_{33}^P \varepsilon_{33}} \frac{\eta\alpha\alpha_m}{\alpha_p + \eta\alpha\alpha_m} \left\{ 1 - \frac{d_{33}^2}{s_{33}^P \varepsilon_{33}} \left[1 - \frac{\eta\alpha\alpha_m}{\alpha_p + \eta\alpha\alpha_m} \right] \right\}^{-1}, \quad (26)$$

where $\eta = \frac{s_{33}^P t_m}{s_{33}^M t_p}$.

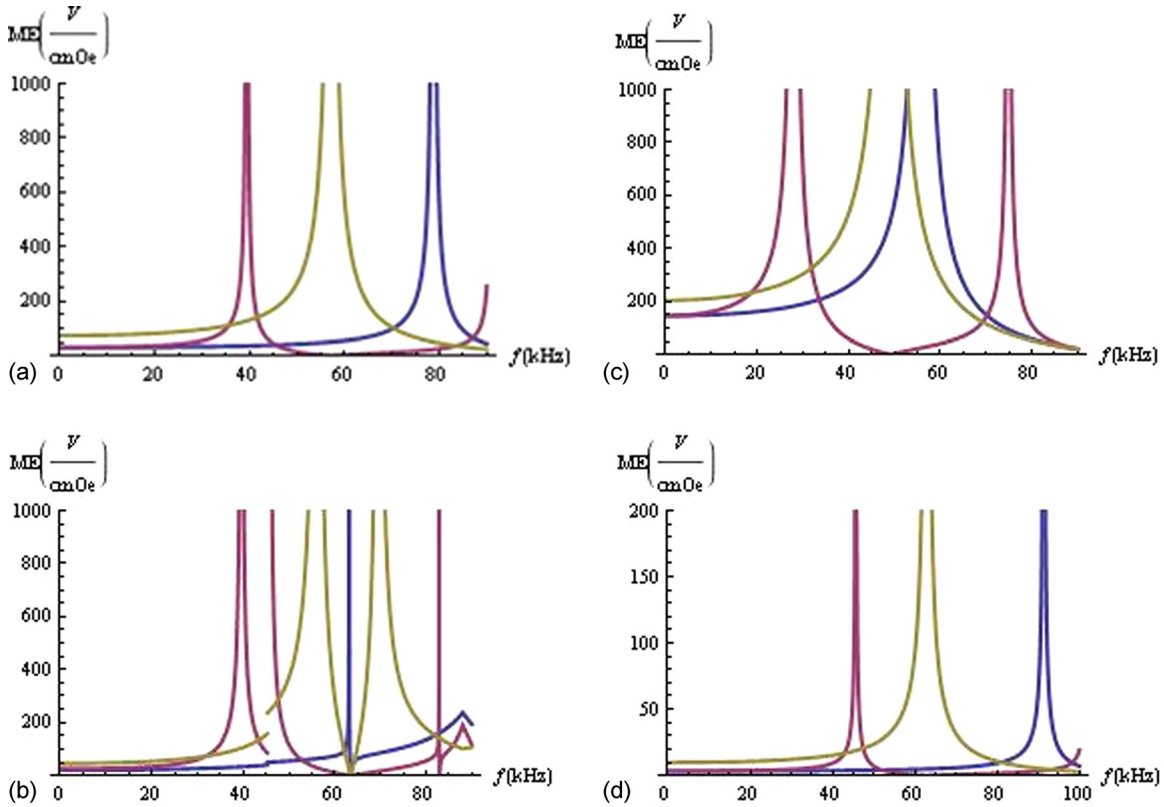

FIG. 2. (a) Locations of first resonant frequencies for three boundary cases. Case (I): blue line, case: (II) purple line, and case (III): green line. Graphs introduced for following parameters: $t_m = 0.02$, $t_p = 0.05$, $2L = 0.04$ m, and $\kappa = 100$. (b) Locations of first resonant frequencies for three boundary cases. Case (I): blue line, case (II): purple line, and case (III): brown line. Graphs introduced for following parameters: $t_m = 0.002$, $t_p = 0.005$, $2L = 0.04$ m, and $\kappa = 0.01$. (c) Locations of first resonant frequencies for three boundary cases. Case (I): blue line, case (II): purple line, and case (III): brown line. Graphs introduced for following parameters: $t_m = 0.02$, $t_p = 0.005$, $2L = 0.04$ m, and $\kappa = 100$. (d) Locations of first resonant frequencies for three boundary cases. Case (I): blue line, case (II): purple line, and case (III): brown line. Graphs introduced for following parameters: $t_m = 0.002$, $t_p = 0.05$, $2L = 0.04$ m, and $\kappa = 100$.

(b) Case of ME coefficients for perfect bonding between layers.

If we assume perfect bonding between layers $\left(\text{i.e., } \frac{G_b}{t_b} \to \infty\right)$, Eqs. (19)–(24) can be simplified. In this case

$$\lambda_1 \to -\zeta^2\omega^2,\ \lambda_2 \to \infty,\ \frac{\tilde{\lambda}_1\tilde{\lambda}_2}{\tilde{\lambda}_1 - \tilde{\lambda}_2} \to 1 + \alpha\eta\alpha_m/\alpha_p,$$
$$\text{where } \zeta^2 = \Omega_p^{-2}\frac{1}{\alpha_p + \eta\alpha\alpha_m}(1 + \alpha\eta\Omega_m^2\Omega_p^{-2}).$$

The ME coefficient in case (I) is then reduced to

$$\alpha_{ME}^I = -\frac{\beta q_{33} d_{33}}{s_{33}^P \varepsilon_{33}}\frac{1}{\Delta_I}\frac{\alpha\eta\alpha_m}{\alpha_p + \alpha\eta\alpha_m}\left\{\frac{tg\omega\varsigma}{\omega\varsigma}\right\}, \quad (27)$$

where $\Delta_I = 1 - \frac{d_{33}^2}{s_{33}^P\varepsilon_{33}}\left\{1 - \frac{\alpha_p}{\alpha_p + \alpha\eta\alpha_m}\frac{tg\omega\varsigma}{\omega\varsigma}\right\}$.

Equation (27) is consistent to that developed in Ref. 21. For frequencies of $\omega = \frac{1}{\varsigma}(\frac{\pi}{2} + \pi k), k = 0, 1, \ldots$, Eq. (27) then simplifies to

$$\alpha_{ME}^I = -\frac{\beta q_{33}}{d_{33}}. \quad (28)$$

From Eq. (28), we can see for a composite made of Metglas and piezoelectric lead zirconium titanate (PZT) layers ($q_{33} = 50 \cdot 10^{-9}$ m/A and $d_{33} = 400 \cdot 10^{-12}$ m/V), the ME coefficient becomes $\alpha_{ME}^I \sim 300$ V/cm Oe, and for a composite made of Permendur and PZT layers, ($q_{33} = 3 \cdot 10^{-9}$ m/A and $d_{33} = 1.7 \cdot 10^{-10}$ m/V) the ME coefficients are equal to $\alpha_{ME}^I \sim 16$ V/cm Oe.

V. NUMERICAL DISCUSSIONS

For calculations, we will make use of the following parameters for Metglas-PZT-Metglas three layer composite:

$$s_{33}^M = 10 \cdot 10^{-12}\,\text{m}^2/\text{N}, \quad q_{33} = 50 \cdot 10^{-9}\,\text{m/A},$$
$$\mu_{33} = \mu_0 \cdot 4.5 \cdot 10^4, \quad \mu_0 = 4\pi \cdot 10^{-7}\,\text{N} \cdot \text{A}^{-2},$$
$$\rho_m = 7180\ \text{kg/m}^3, \quad s_{33}^P = 15.3 \cdot 10^{-12}\,\text{m}^2/\text{N},$$
$$d_{33} = 400 \cdot 10^{-12}\,\text{m/V}, \quad \varepsilon_{33} = 1750 \cdot \varepsilon_0,$$
$$\rho_p = 7600\ \text{kg/m}^3, \quad \varepsilon_0 = 8.9 \cdot 10^{-12}\ \text{F/m}.$$

We will also assume a laminate length $L = 40$ mm and the demagnetization coefficient $\beta = 1$. The behavior of the ME coefficients α_{ME}^i $(i = I, II, III)$ was then calculated in terms of the following parameters: a nondimensional frequency $\Omega = \omega/\Omega_p$, the relative thicknesses of magnetostrictive and piezoelectric layers t_m and t_p, and the rigidity coefficient $\kappa = \frac{G_b s_{33}^M}{t_b}$. Figures 2–5 show the predicted dependence of α_{ME}^i $(i = I, II, III)$ calculated using Eqs. (19)–(24) for different values of the parameters $\Omega = \omega/\Omega_p$, t_m, t_p, and $\kappa = \frac{G_b s_{33}^M}{t_b}$. From these figures, we can see that

- Boundary conditions have significant influence on resonant frequency of the ME coefficient. For case (I), the resonant frequency was about 80 kHz, for case (II), it was about 40 kHz, and for case (III), it was about frequency 57 kHz [see Figs. 2(a)–2(d)].
- Comparisons of Figs. 2(a) and 2(b) show that the rigidity parameter κ not only changes the magnitude of the ME coefficient but also the location of the resonant frequency.
- The thickness parameters t_m and t_p strongly influence the location of the ME resonance frequency [see Figs. 2(c) and 2(d)] and also the 3D representation of the ME coefficient [see Figs. 3(a) and 3(b)].
- The strain distribution is strongly inhomogeneous in the layers. There are strong end effects [see Figs. 4(a)–4(d)]. The strain distribution is strongly influenced by frequency, thickness of the layers, and the rigidity parameter.
- Figures 4(c) and 4(d) show for certain values of the frequency and other parameters that the strain becomes large in magnitude and has an oscillatory type of distribution. This means that a linear theory is not completely suitable to applications describing ME interactions.
- For an ac magnetic field of frequency $\omega_{0*} = \sqrt{\alpha\beta_p\Omega_p^2 + \beta_m\Omega_m^2}$, the ME coefficient is not continuous

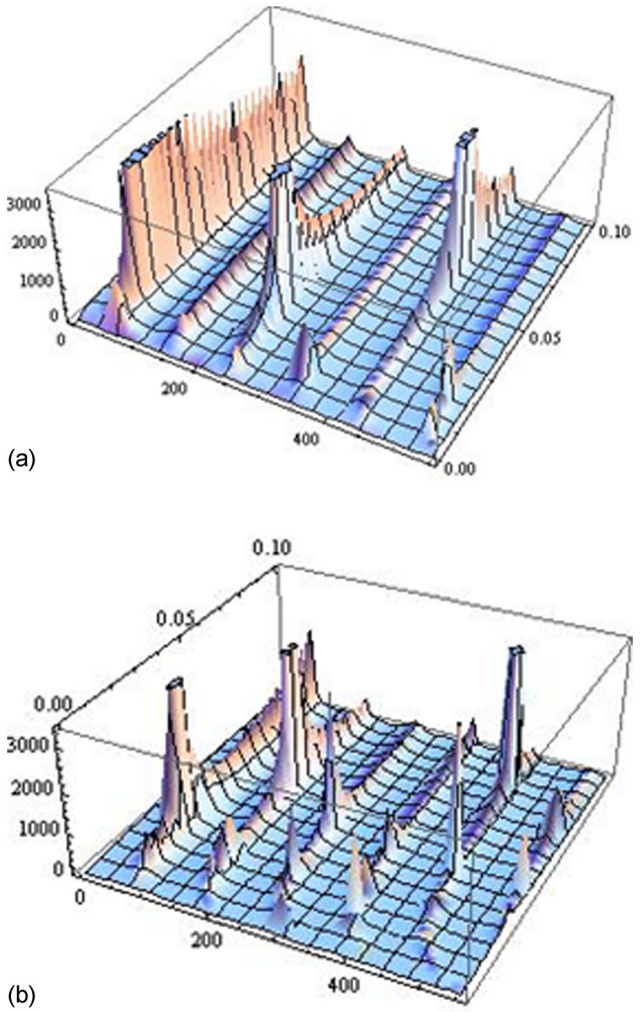

FIG. 3. (a) 3D dependence of ME coefficient α_{ME} on frequency and thickness of magnetic layer t_m. The other parameters chosen as $\kappa = 100$, $t_p = 0.005$, $2L = 0.04$ m: case (I). (b) 3D dependence of ME coefficient α_{ME} on frequency and thickness of magnetic layer t_m. The other parameters chosen as $\kappa = 100$, $t_p = 0.01$, $2L = 0.04$ m: case (I).

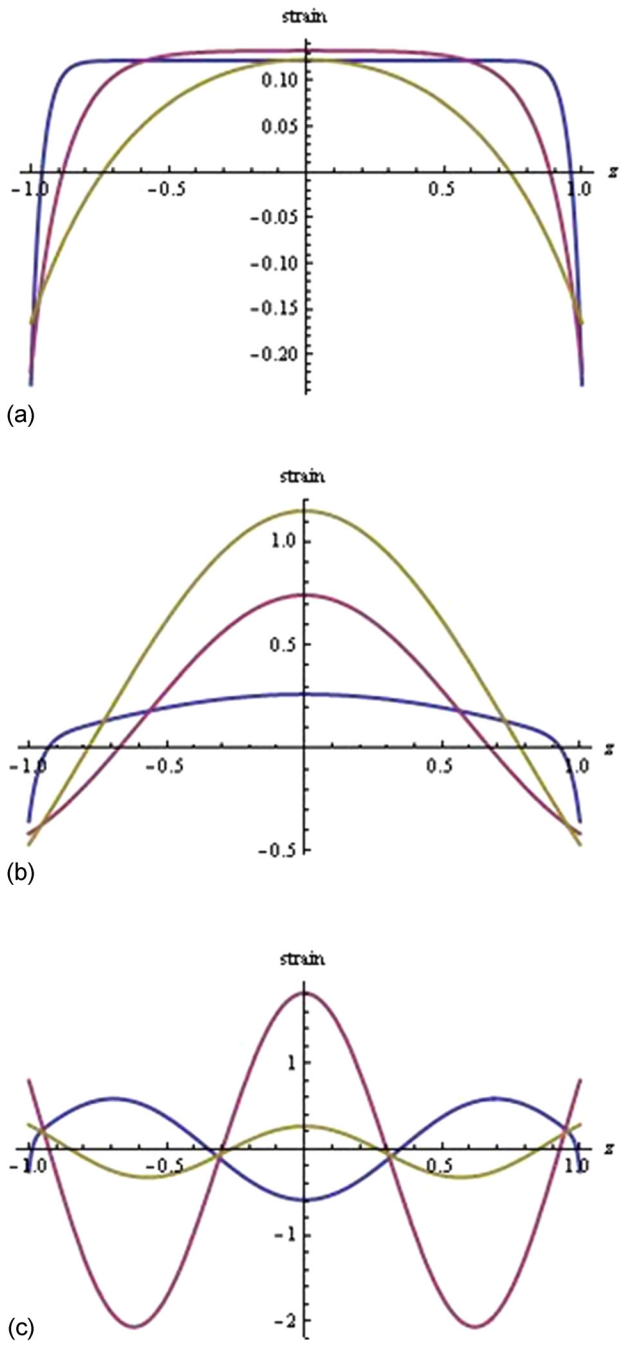

FIG. 4. (a) Strain distribution in piezoelectric for different values of rigidity parameters and $t_m = 0.002$, $t_p = 0.005, 2L = 0.04\,m, \Omega = \frac{\omega}{\Omega_p} = 0$. Blue line $\kappa = 10$; purple line $\kappa = 0.02$, and green line $\kappa = 0.01$. (b) Strain distribution in piezoelectric for different values of rigidity parameters and $t_m = 0.02$, $t_p = 0.05, 2L = 0.04\,m, \Omega = \frac{\omega}{\Omega_p} = 5$. Blue line $\kappa = 10$; purple line $\kappa = 0.02$, and green line $\kappa = 0.01$. (c) Strain distribution in piezoelectric for different values of rigidity parameters and $t_m = 0.02$, $t_p = 0.05$, $2L = 0.04\,m$, $\Omega = \frac{\omega}{\Omega_p} = 50$. Blue line $\kappa = 10$; purple line $\kappa = 0.02$, and green line $\kappa = 0.01$.

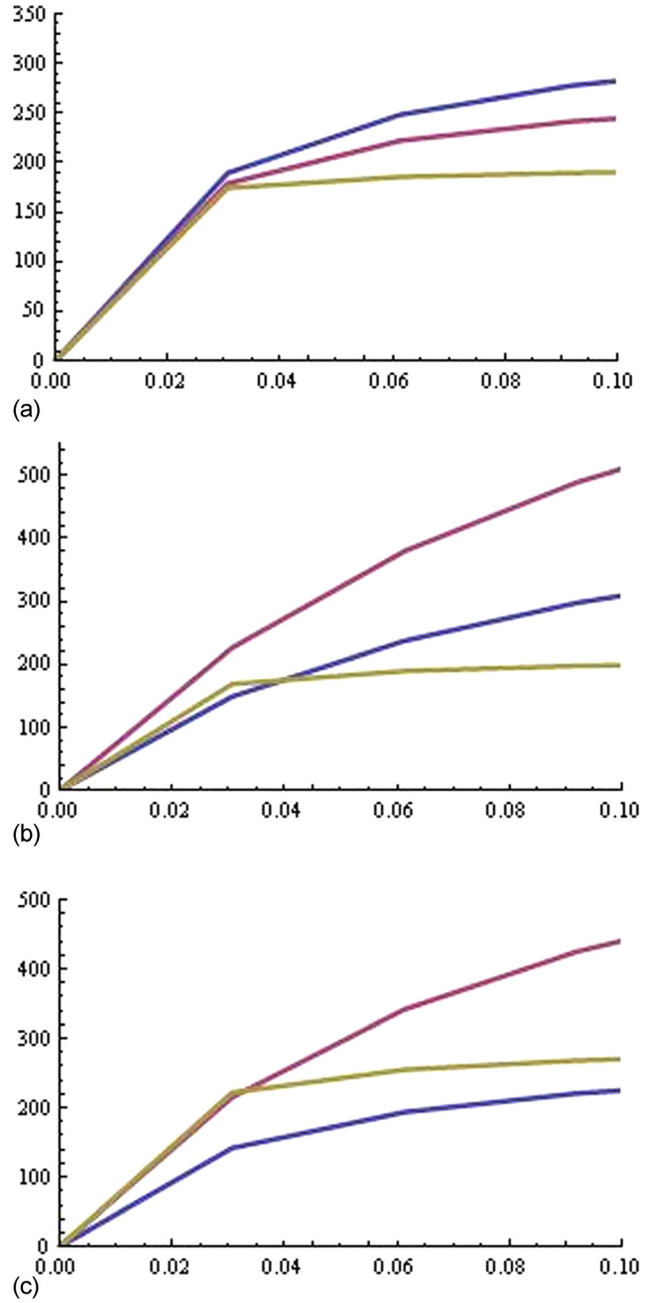

FIG. 5. (a) Distribution of ME coefficient on thickness of magnetic layer t_m. Case (I): blue line; case (II): purple line, and case (III): green line. Graphs introduced for following parameters: $t_p = 0.01$, $2L = 0.04\,m, \Omega = \frac{\omega}{\Omega_p} = 20$, $\kappa = 0.01$. (b) Distribution of ME coefficient on thickness of magnetic layer t_m. Case (I): blue line; case (II): purple line, and case (III): green line. Graphs introduced for following parameters: $t_p = 0.01$, $2L = 0.04\,m$, $\Omega = \frac{\omega}{\Omega_p} = 20, \kappa = 0.1$. (c) Distribution of ME coefficient on thickness of magnetic layer t_m. Case (I): blue line; case (II): purple line, and case (III): green line. Graphs introduced for following parameters: $t_p = 0.01$, $2L = 0.04\,m$, $\Omega = \frac{\omega}{\Omega_p} = 20, \kappa = 100$.

(i.e., the ME coefficient jumps from one value to another [see Fig. 2(b) near 45 kHz]).

- The dependence of the ME coefficient on thickness of the magnetic layer at low frequencies is shown on Figs. 5(a)–5(c). From these figures, we can see that for $\kappa = \frac{G_b s_{33}^M}{t_b} > 0.1$, highest values of the low frequency ME coefficient occur for case (II) (i.e., cantilever beam-layers).

VI. CONCLUSIONS

An analytical model, including dynamic shear-lag effect has been proposed for magneto-electric laminate composites. The theory is applied to Metglas-PZT-Metglas tri-layer composite structures. The frequency dependence of the ME coefficient predicts that the resonance depends strongly on the physical and geometrical parameters of the laminates.

Nondimensional shear lag parameter κ, frequency $\Omega = \omega/\Omega_p$, and relative thicknesses of magnetostrictive and piezoelectric layers t_m and t_p were used to study the influences caused by material properties and sample geometries on the ME coefficient. The results indicate that shear lag causes substantial strain inhomogeneity near free ends. For certain values of frequency, the distribution of strain becomes large and results in an oscillatory behavior, which makes questionable a linear theory for ME interactions. We then show, when the value of the ac magnetic field frequency equals $\omega_{0*} = \sqrt{\alpha\beta_p\Omega_p^2 + \beta_m\Omega_m^2}$, the ME coefficient is not continuous but rather jumps from one value to another.

ACKNOWLEDGMENTS

This work was sponsored by the DARPA and the Office of Naval Research.

[1]M. Fiebig, J. Phys. D: Appl. Phys. **38**, R123 (2005).
[2]C. W. Nan, M. I. Bichurin, S. X. Dong, D. Viehland, and G. Srinivasan, J. Appl. Phys. **103**, 031101 (2008).
[3]S. X. Dong, J. Y. Zhai, J. F. Li, and D. Viehland, Appl. Phys. Lett. **89**, 252904 (2006).
[4]S. X. Dong, J. Y. Zhai, Z. P. Xing, J. F. Li, and D. Viehland, Appl. Phys. Lett. **91**, 022915 (2007).
[5]M. Bichurin, V. Petrov, and G. Srinivasan, Phys. Rev. B **68**, 054402 (2003).
[6]J. Ryu, A. V. Carazo, K. Uchino, and H. E. Kim, J. Electroceram. **7**, 17 (2001).
[7]C. W. Nan, L. Liu, N. Cai, J. Zhai, Y. Ye, Y. H. Lin, L. J. Dong, and C. X. Xiong, Appl. Phys. Lett. **81**, 3831 (2002).
[8]M. I. Bichurin, V. M. Petrov, S. V. Averkin, and E. Liverts, J. Appl. Phys. **107**, 053904 (2010).
[9]G. Srinivasan, E. T. Rasmussen, B. J. Levin, and R. Hayes, Phys. Rev. B **65**, 134402 (2002).
[10]S. Priya, R. Islam, S. X. Dong, and D. Viehland, J. Electroceram. **19**, 149–166 (2007).
[11]S. X. Dong, J. F. Li, and D. Viehland, Philos. Mag. Lett. **83**, 769 (2003).
[12]G. Harshe, J. P. Dougherty, and R. E. Newnham, Int. J. Appl. Electromagn. Mater. **4**, 145 (1993).
[13]M. I. Bichurin, V. M. Petrov, and G. Srinivasan, J. Appl. Phys. **92**, 7681 (2002).
[14]D. A. Filippov, M. I. Bichurin, V. M. Petrov, V. M. Laletin, and G. Srinivasan, Phys. Solid State **46**, 1674 (2004).
[15]M. I. Bichurin, V. M. Petrov, O. V. Ryabkov, S. V. Averkin, and G. Srinivasan, Phys. Rev. B **72**, 060408(R) (2005).
[16]E. F. Crawley and J. Deluis, AIAA J. **25**, 1373 (1987).
[17]C.-M. Chang and G. Carman, Phys. Rev. B **76**, 134116 (2007).
[18]V. Z. Parton and B. A. Kudryavtsev, *Electromagnetoelasticity: Piezoelectricsand Electrically Conductive Solids* (Gordon and Breach Science, New York, 1988).
[19]N. N. Rogacheva, J. Appl. Math. Mech. **74**, 721 (2010).
[20]A. Aharoni, J. Appl. Phys. **83**, 3432 (1998).
[21]D. A. Filippov, G. Srinivasan, and A. Gupta, J. Phys.: Condens. Matter **20**, 425206 (2008).